PCCP

PAPER

Cite this: *Phys. Chem. Chem. Phys.*, 2016, **18**, 2730

Single-molecule insight into Wurtz reactions on metal surfaces†

Qiang Sun, Liangliang Cai, Yuanqi Ding, Honghong Ma, Chunxue Yuan and Wei Xu*

Received 23rd October 2015, Accepted 11th December 2015

DOI: 10.1039/c5cp06459g

www.rsc.org/pccp

Wurtz reactions feature the dehalogenated coupling of alkyl halides. In comparison to their widely investigated counterparts, Ullmann reactions, Wurtz reactions have however been scarcely explored on surfaces. Herein, by combining high-resolution STM imaging and DFT calculations, we have systematically investigated Wurtz reactions on three chemically different metal surfaces including Cu(110), Ag(110) and Au(111). We find that the Wurtz reactions could be achieved on all three surfaces, and the temperatures for triggering the reactions are in the order of Cu(110) > Ag(110) > Au(111). Moreover, DFT calculations have been performed to unravel the pathways of on-surface Wurtz reactions and identify three basic steps of the reactions including debromination, diffusion and coupling processes. Interestingly, we found that the mechanism of the on-surface Wurtz reaction is intrinsically different from the Ullmann reaction and it is revealed that the coupling process is the rate-limiting step of Wurtz reactions on three different substrates. These findings have given a comprehensive picture of Wurtz reactions on metal surfaces and demonstrated that such a reaction could be an alternative reaction scheme for advanced on-surface synthesis.

Introduction

Recently, on-surface synthesis has gained considerable attention due to the prospects for (1) constructing versatile nanostructures with efficient electron transportability and high stability for (opto)electronics applications, (2) unraveling the mechanisms of well-known chemical reactions by single-molecule-resolved real-space surface methods, (3) and moreover exploring new chemistry.[1–3] For example, various well-known chemical reactions including Ullmann reactions,[4–10] Bergman cyclization,[11,12] click reactions,[13,14] Glaser coupling,[15,16] imine formation[17] and Sonogashira reactions,[18] as well as some unexpected reactions such as decarboxylative polymerization,[19] dehydrogenative homocoupling of alkane, alkene, and arene[20–24] have been achieved and investigated on different surfaces. Wurtz reactions, which are a dehalogenated coupling of alkyl halides, have long been discovered in solution chemistry[25] and often used in hydrocarbon preparation and polymer synthesis, which usually need Na as a catalyst.[26,27] As compared to their counterparts, Ullmann reactions, a dehalogenated coupling of aryl halides, Wurtz reactions have however been scarcely investigated on surfaces. It is therefore of particular interest to introduce Wurtz reactions on surfaces and gain fundamental insight into these reactions at the single-molecule level.

In this study, we choose an organic molecule which has a bromomethyl group functionalized on a biphenyl backbone (shortened as BMBP), as indicated in Scheme 1. Three kinds of single-crystal metal surfaces Cu(110), Ag(110), Au(111) have been selected to investigate the feasibility of on-surface Wurtz reactions.[28–30] By combining submolecularly resolved scanning tunneling microscopy (STM) imaging and density functional theory (DFT) calculations, we have systematically investigated

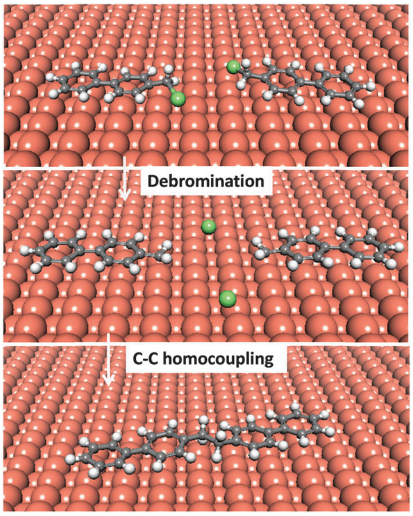

Scheme 1 On-surface Wurtz reaction of BMBP molecules on Cu(110) *via* a debrominated intermediate. Carbon: grey, hydrogen: white, bromine: green, copper: brown.

Tongji-Aarhus Joint Research Center for Nanostructures and Functional Nanomaterials, College of Materials Science and Engineering, Tongji University, Caoan Road 4800, Shanghai 201804, P. R. China. E-mail: xuwei@tongji.edu.cn

† Electronic supplementary information (ESI) available. See DOI: 10.1039/c5cp06459g

the Wurtz reactions of BMBP on three different metal surfaces, and successfully triggered dehalogenated homocoupling of BMBP molecules on these surfaces. The single-molecule-resolution STM images further allow us to identify the debrominated intermediates and unravel the step-by-step reaction pathways. Interestingly, in comparison to the on-surface Ullmann reaction, the debromination process of Wurtz reactions is more facile to occur, and no metal-mediated intermediate is observed. Moreover, detailed DFT-based transition-state searches have been performed to determine the energy barriers of the basic steps of Wurtz reactions including C–Br bond scission, radical diffusion and homocoupling processes on three substrates. It is noticeable that the coupling process is the rate-limiting step of on-surface Wurtz reactions, which is intrinsically different from Ullmann reactions. These findings thus demonstrate the feasibility of introducing Wurtz reactions on metal surfaces, which may provide an alternative reaction scheme for on-surface synthesis of hydrocarbons and other related novel nanostructures.

Experimental

Sample preparation and STM experiments

The STM experiments were performed in an UHV chamber with a base pressure of 1×10^{-10} mbar. The system is equipped with a variable-temperature "Aarhus-type" scanning tunneling microscope,[31,32] a molecular evaporator, and standard facilities for sample preparation. The metal substrates were prepared by several cycles of 1.5 keV Ar^+ sputtering followed by annealing resulting in clean and flat terraces separated by monatomic steps. After the system was thoroughly degassed, the BMBP molecules (purchased from Tokyo Chemical Industry Co., Ltd purity >98%) were deposited at ∼293 K onto the substrates. The sample was thereafter transferred within the UHV chamber to the microscope, where measurements were carried out in a typical temperature range of 100–150 K.

DFT calculations

All of the calculations were performed in the framework of DFT by using the Vienna Ab Initio Simulation Package (VASP).[33,34] The projector augmented wave method was used to describe the interaction between ions and electrons.[35,36] We employed the Perdew–Burke–Ernzerhof generalized gradient approximation exchange–correlation functional,[37] and van der Waals (vdW) interactions were included using the dispersion corrected DFT-D2 method of Grimme.[38] The atomic structures were relaxed using the conjugate gradient algorithm scheme as implemented in the VASP until the forces on all unconstrained atoms were ≤ 0.03 eV $Å^{-1}$ for geometry optimization. The simulated STM image was obtained using the Tersoff–Hamann method,[39] in which the local density of states (LDOS) is used to approximate the tunneling current. The climbing-image nudged elastic band was applied to locate the transition state[40] and the reaction pathway was optimized until the forces acting on the path were converged typically to ≤ 0.05 eV $Å^{-1}$. Eight images were used to locate the transition state in the CI-NEB calculations, and the shapes of the energy curves are determined from the calculations.

Results and discussion

As shown in Fig. 1a, after the deposition of BMBP molecules on Cu(110) held at ∼230 K, we observe the formation of close-packed nanostructures composed of rod-like features and bright protrusions, which are assigned to the debrominated BMBP (BMBP*) molecules and detached Br atoms.[41,42] No intact BMBP molecule is observed at even lower substrate temperature (∼150 K) (Fig. S1, ESI†), which implies that the energy barrier for the C–Br bond scission of alkyl bromide on the surface is quite low. Note that the deposition of the BMBP molecules was at ∼293 K, so it seems to be impossible that the BMBP molecules are already debrominated at the crucible. Comparing the DFT optimized model and the corresponding simulated STM image of BMBP* and Br atoms on Cu(110) with the experimental findings (Fig. 1b and c), a good agreement is achieved. From the model we could identify that the BMBP* molecule is stabilized by interacting with substrate copper atoms. Interestingly, after further annealing the sample to ∼450 K for 10 minutes, we find that the BMBP* molecules dimerize and form self-assembled nanostructures with Br atoms on the surface as shown in Fig. 1d. Comparing the DFT optimized model and the corresponding simulated STM image of the BMBP* dimer with the experimental findings (Fig. 1e and f), a good agreement is achieved. Moreover, homocoupling of BMBP*

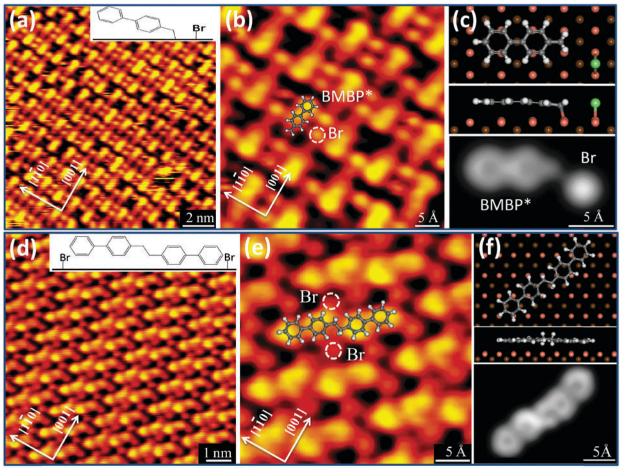

Fig. 1 (a) Large-scale and (b) close-up STM images showing debromination of BMBP molecules right after deposition on Cu(110) below room temperature (∼230 K). A scaled model of the debrominated BMBP (as BMBP* in the following) is overlaid on the corresponding STM image, and a detached Br atom is indicated by a dashed circle in (b). (c) Top and side views of the DFT optimized model of a BMBP* molecule together with the detached Br atom on Cu(110), as well as the corresponding simulated STM image. (d) Large-scale and (e) close-up STM images showing homocoupling of BMBP* molecules after annealing the sample to ∼450 K. A scaled model of a BMBP* dimer is overlaid on the corresponding STM image, and detached Br atoms are indicated by dashed circles in (e). (f) Top and side views of the DFT optimized model of a BMBP* dimer on Cu(110), and the corresponding simulated STM image. Scanning conditions: I_t = 0.90 nA, V_t = −1750 mV.

molecules is evidenced by moving the dimer structure as a whole with lateral STM manipulations (Fig. S2, ESI†).[43,44] It is worth noting that the debrominated intermediate BMBP* is stabilized on Cu(110) for Wurtz reactions, and we do not find the C–Cu–C organometallic intermediate which is normally present in Ullmann reactions on copper surfaces.[45–47]

We have also performed experiments on Ag(110) to explore the generality of on-surface Wurtz reactions and the influence of different metal substrates on these reactions. As shown in Fig. 2a, similar to the case of Cu(110), debromination of BMBP also occurs after deposition on Ag(110) at low temperatures (~150–200 K). Good agreement is also achieved by comparing the DFT optimized model and the corresponding simulated STM image of BMBP* and Br atoms on Ag(110) with the experimental STM image (Fig. 2b and c). Interestingly, further annealing the sample to ~420 K for 10 minutes (lower than that on Cu(110)) results in the dimerization of BMBP* molecules on the surface as shown in Fig. 2d. Comparing the DFT optimized model and the corresponding simulated STM image of the BMBP* dimer with the experimental STM image (Fig. 2e and f), a good agreement is achieved. Note that we still do not find the evidence of C–Ag–C organometallic intermediates.[46,48]

In the next step, we move to a chemically even less reactive surface Au(111). As shown in Fig. 3a and b, unexpectedly, debromination of BMBP also occurs right after deposition on Au(111) at low temperatures (~150–200 K), which is substantiated by the DFT optimized model and the corresponding simulated STM image (Fig. 3c). The debrominated molecules show higher mobility on Au(111) as observed from the fuzzy regions of the STM-image (Fig. 3a). More interestingly, a gentle thermal treatment to ~350 K for 10 minutes (lower than that for both Cu(110) and Ag(110)) results in the dimerization of BMBP* molecules on the surface as shown in Fig. 3d and e. The DFT optimized model and the corresponding simulated STM image have also been shown in Fig. 3f. Likewise, no C–Au–C organometallic intermediate is observed.[6] Note that the annealing temperatures are the onset temperatures for triggering the coupling reactions on the surfaces. By comparing the Wurtz reaction of BMBP on three chemically different substrates, it is seen that: (1) debromination of BMBP on all three substrates could be easily achieved at relatively low temperatures (~150–200 K); (2) the debrominated intermediate BMBP* is observed on three substrates; (3) the temperatures for triggering Wurtz reactions on three substrates are in the order of Cu(110) > Ag(110) > Au(111). We have not found the cis-configuration dimer on three surfaces, which is probably because it is energetically unfavorable than the trans-configuration one.

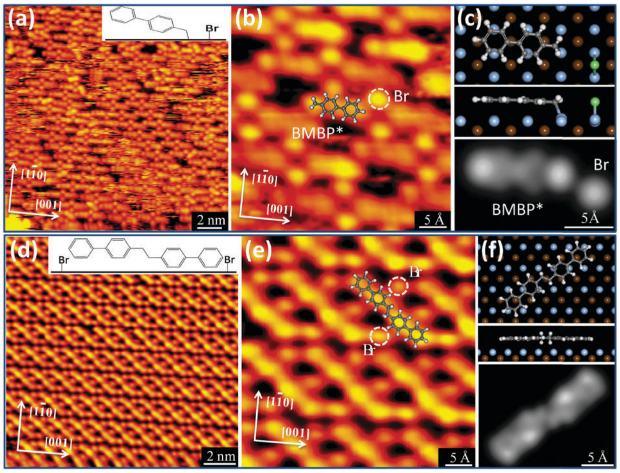

Fig. 2 (a) Large-scale and (b) close-up STM images showing debromination of BMBP molecules right after deposition on Ag(110). A scaled model of BMBP* is overlaid on the corresponding STM image, and a detached Br atom is indicated by a dashed circle in (b). (c) Top and side views of DFT optimized model of a BMBP* molecule together with the detached Br atom on Ag(110), and the corresponding simulated STM image. (d) Large-scale and (e) close-up STM images showing homocoupling of BMBP* molecules after annealing the sample to ~420 K. A scaled model of a BMBP* dimer is overlaid on the corresponding STM image, and detached Br atoms are indicated by dashed circles in (e). (f) Top and side views of the DFT optimized model of a BMBP* dimer on Ag(110), and the corresponding simulated STM image. Scanning conditions: I_t = 1.2 nA, V_t = −1000 mV.

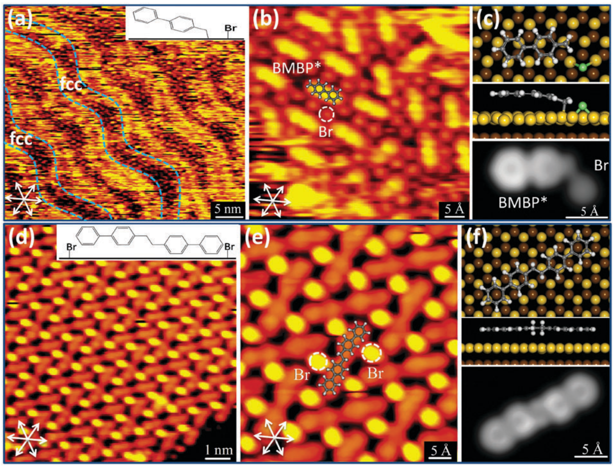

Fig. 3 (a) Large-scale and (b) close-up STM images showing debromination of BMBP molecules right after deposition on Au(111) below room temperature. The BMBP* molecules mainly adsorb at fcc-regions of the herringbone reconstructions as indicated by the blue dashed lines in (a). A scaled model of BMBP* is overlaid on the corresponding STM image, and a detached Br atom is indicated by a dashed circle in (b). (c) Top and side views of the DFT optimized model of a BMBP* molecule together with the detached Br atom on Au(111), and the corresponding simulated STM image. (d) Large-scale and (e) close-up STM images showing homocoupling of BMBP* molecules after annealing the sample to ~350 K. A scaled model of a BMBP* dimer is overlaid on the corresponding STM image, and detached Br atoms are indicated by dashed circles in (e). (f) Top and side views of the DFT optimized model of a BMBP* dimer on Au(111), and the corresponding simulated STM image. Scanning conditions: I_t = 0.9 nA, V_t = −1750 mV.

The unexpected experimental findings (as compared with on-surface Ullmann reactions) have aroused our further interest to elucidate the scenarios of on-surface Wurtz reactions. We thus carry out systematic DFT calculations to search the reaction pathways by using the nudged elastic band (NEB) method. Generally, the on-surface dehalogenated homocoupling is associated with three fundamental reaction steps: (a) dehalogenation of the molecular precursors; (b) diffusion of the dehalogenated molecules; (c) coupling between the dehalogenated molecules. All these steps

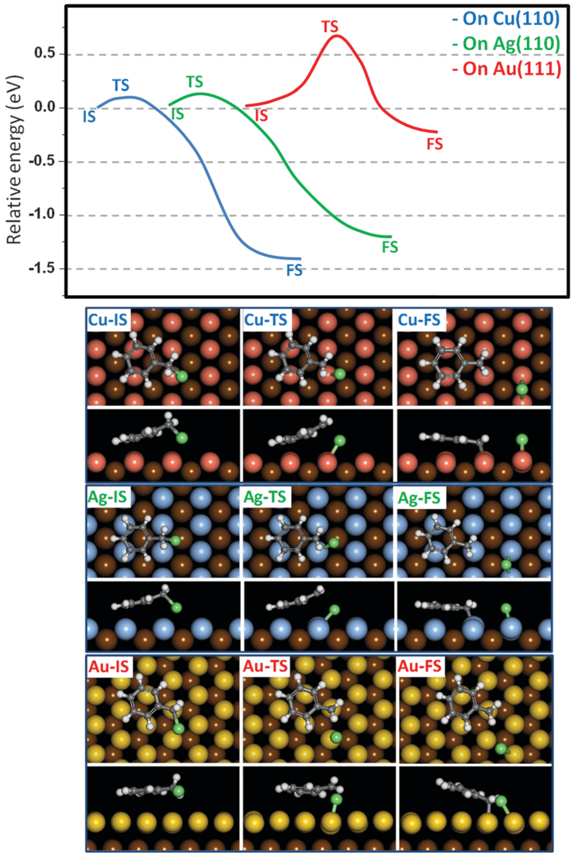

Fig. 4 DFT-calculated energy diagrams for the C–Br scission of bromomethylbenzene (BMB) on three different substrates. The structural models of the initial states (ISs), the transition states (TSs) and the final states (FSs) along the pathways are shown below.

crucially depend on the underlying substrate.[28] Note that all of the experiments have been performed with different molecular coverages (<1 monolayer), and the experimental observations of the homocoupling reactions on three surfaces are almost the same. Firstly, as illustrated in Fig. 4a, we plot the energy diagrams of C–Br scission of bromomethylbenzene (BMB) on three substrates to determine the energy barriers ($E_{\mathrm{barrier}} = E_{\mathrm{TS}} - E_{\mathrm{IS}}$) and the reaction energies ($E_{\mathrm{react}} = E_{\mathrm{FS}} - E_{\mathrm{IS}}$). The debromination is more favorable on Cu(110) (with a E_{barrier} of 0.073 eV) than that on Ag(110) (with a E_{barrier} of 0.107 eV) and Au(111) (with a E_{barrier} of 0.663 eV), which suggests that Cu(110) is the most reactive surface for dehalogenation among these three surfaces. Moreover, the debromination reaction on Cu(110) is more exothermic than those on the other two surfaces. Note that the debromination barrier of BMBP on Au(111) is a bit higher than the experimental condition (~150–200 K), which may be caused by some factors including herringbone reconstruction and gold atoms that are not taken into account due to the substantial computational efforts.

A step further, to test if the surface mobility of the debrominated species limits the on-surface Wurtz reaction,[49] we plot the energy diagrams of the diffusion of the debrominated BMB (BMB*) molecule on three different substrates. As shown in Fig. 5, it is more favorable for the BMB* molecule to diffuse along the [1$-$10] direction than the [001] direction on both Cu(110) and Ag(110), which is probably due to the smaller lattice distances.[50] Overall, the diffusion barriers of BMB* molecules on all three substrates are not that large and the molecules could freely move around on the surfaces at room temperature. So the diffusion processes are not the rate-limiting steps for Wurtz reactions on

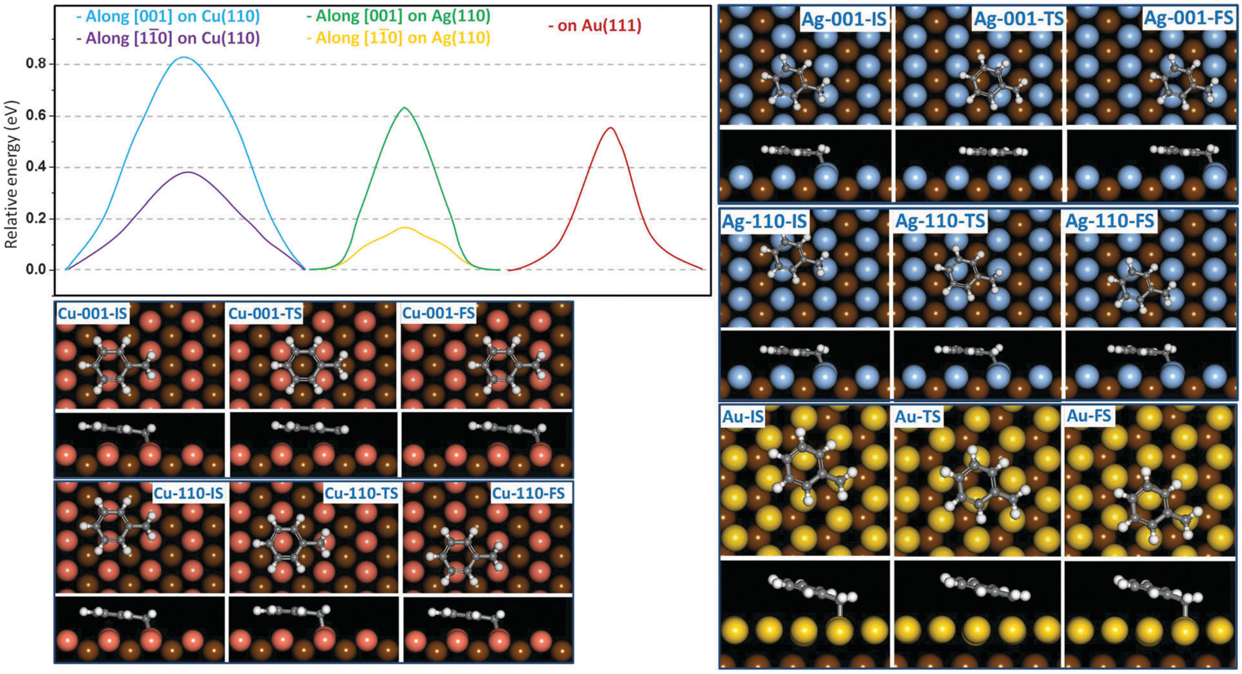

Fig. 5 DFT-calculated energy diagrams for diffusion of the debrominated BMB on three different substrates. Due to the anisotropy of the Cu(110) and Ag(110) substrates, two pathways along their high-symmetry directions are searched, respectively. The structural models of the initial states (ISs), the transition states (TSs) and the final states (FSs) along the pathways are shown.

these three surfaces. As compared to on-surface Ullmann reactions, we believe that the absence of a metal-mediated intermediate is due to the relatively strong interactions between the debrominated species and the substrates.

Finally, we explore the coupling reaction of two debrominated species on three substrates. As shown in Fig. 6, the energy barriers of coupling processes are obviously higher than those of debromination and diffusion processes on the surfaces, which indicates that the coupling processes are the rate-limiting steps of Wurtz reactions on the surfaces. As seen that the coupling of debrominated BMB molecules is energetically most favorable on Au(111) and least favorable on Cu(110), which is in good agreement with the experimental conditions (required temperatures) for triggering the on-surface Wurtz reactions. Moreover, the coupling process on Au(111) is most exothermic among three surfaces. As illustrated from the molecular configurations along the pathways on three surfaces, we identify that it is necessary to lift one of the hydrogen atoms on the methyl groups to complete the coupling reactions, which accounts for the relatively high energy barriers compared to debromination and diffusion processes. Note that the lattice plane of Au(111) is different from those of Cu(110) and Ag(110). So, the initial configuration of the homocoupling from two debrominated species on Au(111) is inevitably distinct from those on Cu(110) and Ag(110).

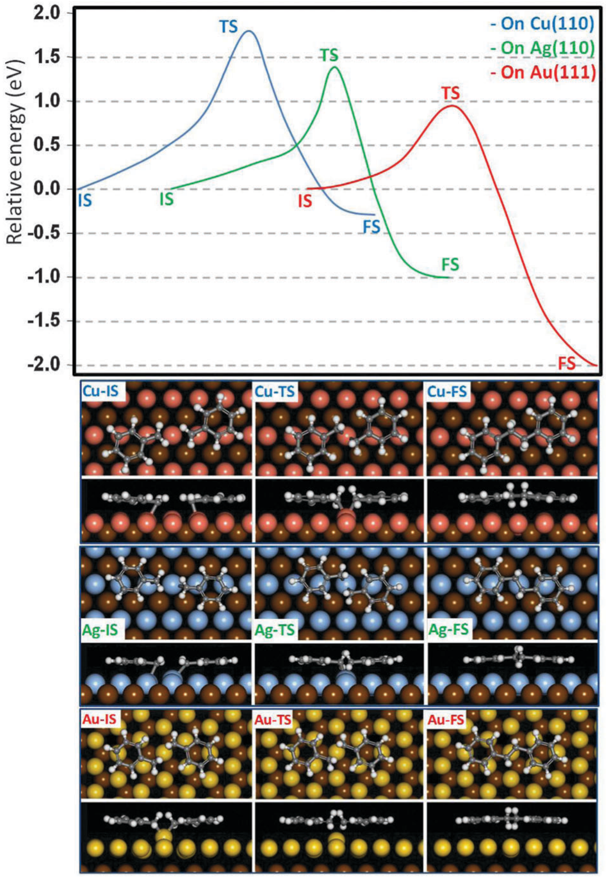

Fig. 6 DFT-calculated energy diagrams for coupling of two debrominated BMB molecules on three different substrates. The structural models of the initial states (ISs), the transition states (TSs) and the final states (FSs) along the pathways are shown.

Conclusions

In conclusion, by combining high-resolution UHV-STM imaging and DFT calculations, we have performed a systematic study of Wurtz reactions on different metal surfaces and compared their different activities.[29,49] Experimentally, we have achieved homocoupling of alkyl halides *via* Wurtz reactions on surfaces, and identified the debrominated intermediates. The temperatures for triggering Wurtz reactions on three surfaces are in the order of Cu(110) > Ag(110) > Au(111), which is consistent with the calculated energy barriers. Moreover, by calculating the whole scenarios of debromination, diffusion and coupling processes the reaction pathways have been revealed. These findings have given a comprehensive picture of Wurtz reactions on different metal surfaces, and illustrated that Wurtz reactions could be a good strategy for on-surface synthesis. Furthermore, it is notable that the underlying mechanisms of dehalogenated homocoupling of C–X groups (X stands for halogen) on surfaces crucially depend on the distinct carbon centers (*e.g.* Ullmann reactions of aryl halides and Wurtz reactions of alkyl halides). Further studies on dehalogenated homocoupling of alkynyl halides and alkenyl halides which are of particular interest and fundamental importance are underway.

Acknowledgements

The authors acknowledge the financial support from the National Natural Science Foundation of China (21103128, 21473123), the Research Fund for the Doctoral Program of Higher Education of China (20120072110045).

Notes and references

1 C. A. Palma and P. Samorì, *Nat. Chem.*, 2011, **3**, 431.
2 G. Franc and A. Gourdon, *Phys. Chem. Chem. Phys.*, 2011, **13**, 14283.
3 J. Bjork and F. Hanke, *Chem. – Eur. J.*, 2014, **20**, 928.
4 J. Cai, P. Ruffieux, R. Jaafar, M. Bieri, T. Braun, S. Blankenburg, M. Muoth, A. P. Seitsonen, M. Saleh, X. Feng, K. Mullen and R. Fasel, *Nature*, 2010, **466**, 470.
5 C. Morchutt, J. Björk, S. Krotzky, R. Gutzler and K. Kern, *Chem. Commun.*, 2015, **51**, 2440.
6 H. Zhang, H. Lin, K. Sun, L. Chen, Y. Zagranyarski, N. Aghdassi, S. Duhm, Q. Li, D. Zhong, Y. Li, K. Müllen, H. Fuchs and L. Chi, *J. Am. Chem. Soc.*, 2015, **137**, 4022.
7 W. Wang, X. Shi, S. Wang, M. A. Van Hove and N. Lin, *J. Am. Chem. Soc.*, 2011, **133**, 13264.
8 L. Grill, M. Dyer, L. Lafferentz, M. Persson, M. V. Peters and S. Hecht, *Nat. Nanotechnol.*, 2007, **2**, 687.
9 J. Eichhorn, D. Nieckarz, O. Ochs, D. Samanta, M. Schmittel, P. J. Szabelski and M. Lackinger, *ACS Nano*, 2014, **8**, 7880.

10 T. Dienel, J. Goméz-Díaz, A. P. Seitsonen, R. Widmer, M. Iannuzzi, H. Sachdev, K. Mullen, J. Hutter and O. Groening, *ACS Nano*, 2014, **8**, 6571.

11 Q. Sun, C. Zhang, Z. Li, H. Kong, Q. Tan, A. Hu and W. Xu, *J. Am. Chem. Soc.*, 2013, **135**, 8448.

12 D. G. de Oteyza, P. Gorman, Y. C. Chen, S. Wickenburg, A. Riss, D. J. Mowbray, G. Etkin, Z. Pedramrazi, H. Tsai, A. Rubio, M. F. Crommie and F. R. Fischer, *Science*, 2013, **340**, 1434.

13 F. Bebensee, C. Bombis, S. R. Vadapoo, J. R. Cramer, F. Besenbacher, K. V. Gothelf and T. R. Linderoth, *J. Am. Chem. Soc.*, 2013, **135**, 2136.

14 D. Arado, H. Monig, H. Wagner, J. H. Franke, G. Langewisch, P. A. Held, A. Studer and H. Fuchs, *ACS Nano*, 2013, **7**, 8509.

15 Y. Q. Zhang, N. Kepcija, M. Kleinschrodt, K. Diller, S. Fischer, A. C. Papageorgiou, F. Allegretti, J. Bjork, S. Klyatskaya, F. Klappenberger, M. Ruben and J. V. Barth, *Nat. Commun.*, 2012, **3**, 1286.

16 H. Y. Gao, H. Wagner, D. Zhong, J. H. Franke, A. Studer and H. Fuchs, *Angew. Chem., Int. Ed.*, 2013, **52**, 4024.

17 S. Weigelt, C. Busse, C. Bombis, M. M. Knudsen, K. V. Gothelf, T. Strunskus, W. Woll, M. Dahlbom, B. Hammer, E. Lægsgaard, F. Besenbacher and T. R. Linderoth, *Angew. Chem., Int. Ed.*, 2007, **46**, 9227.

18 C. Sanchez-Sanchez, N. Orozco, J. P. Holgado, S. K. Beaumont, G. Kyriakou, D. J. Watson, A. R. Gonzalez-Elipe, L. Feria, J. F. Sanz and R. M. Lambert, *J. Am. Chem. Soc.*, 2015, **137**, 940.

19 H. Y. Gao, P. A. Held, M. Knor, C. Mück-Lichtenfeld, J. Neugebauer, A. Studer and H. Fuchs, *J. Am. Chem. Soc.*, 2014, **136**, 9658.

20 D. Zhong, J. Franke, S. K. Podiyanachari, T. Blçmker, H. Zhang, G. Kehr, G. Erker, H. Fuchs and L. Chi, *Science*, 2011, **334**, 213.

21 M. Int Veld, P. Iavicoli, S. Haq, D. B. Amabilino and R. Raval, *Chem. Commun.*, 2008, 1536.

22 Q. Sun, C. Zhang, H. Kong, Q. Tan and W. Xu, *Chem. Commun.*, 2014, **50**, 11825.

23 A. Wiengarten, K. Seufert, W. Auwarter, D. Ecija, K. Diller, F. Allegretti, F. Bischoff, S. Fischer, D. A. Duncan, A. C. Papageorgiou, F. Klappenberger, R. G. Acres, T. H. Ngo and J. V. Barth, *J. Am. Chem. Soc.*, 2014, **136**, 9346.

24 Q. Sun, L. Cai, Y. Ding, L. Xie, C. Zhang, Q. Tan and W. Xu, *Angew. Chem., Int. Ed.*, 2015, **54**, 4549.

25 A. Wurtz, *Ann. Chim. Phys.*, 1855, **44**, 275.

26 R. L. Letsinger, *J. Am. Chem. Soc.*, 1948, **70**, 406.

27 N. Devylder, M. Hill, K. C. Molloy and G. J. Price, *Chem. Commun.*, 1996, 711.

28 J. Bjork, F. Hanke and S. Stafström, *J. Am. Chem. Soc.*, 2013, **135**, 5768.

29 M. Bieri, M. T. Nguyen, O. Gröning, J. Cai, M. Treier, K. Ait-Mansour, P. Ruffieux, C. A. Pignedoli, D. Passerone, M. Kastler, K. Müllen and R. Fasel, *J. Am. Chem. Soc.*, 2010, **132**, 16669.

30 R. Gutzler, H. Walch, G. Eder, S. Kloft, W. M. Heckl and M. Lackinger, *Chem. Commun.*, 2009, 4456–4458.

31 F. Besenbacher, *Rep. Prog. Phys.*, 1996, **59**, 1737.

32 E. Lægsgaard, L. Osterlund, P. Thostrup, P. B. Rasmussen, I. Stensgaard and F. Besenbacher, *Rev. Sci. Instrum.*, 2001, **72**, 3537.

33 G. Kresse and J. Hafner, *Phys. Rev. B: Condens. Matter Mater. Phys.*, 1993, **48**, 13115.

34 G. Kresse and J. Furthmuller, *Phys. Rev. B: Condens. Matter Mater. Phys.*, 1996, **54**, 11169.

35 P. E. Blöchl, *Phys. Rev. B: Condens. Matter Mater. Phys.*, 1994, **50**, 17953.

36 G. Kresse and D. Joubert, *Phys. Rev. B: Condens. Matter Mater. Phys.*, 1999, **59**, 1758.

37 J. P. Perdew, K. Burke and M. Ernzerhof, *Phys. Rev. Lett.*, 1996, **77**, 3865.

38 S. Grimme, *J. Comput. Chem.*, 2006, **27**, 1787.

39 J. Tersoff and D. R. Hamann, *Phys. Rev. B: Condens. Matter Mater. Phys.*, 1985, **31**, 805.

40 G. Henkelman, B. P. Uberuaga and H. Jonsson, *J. Chem. Phys.*, 2000, **113**, 9901.

41 M. Di Giovannantonio, M. El Garah, J. Lipton-Duffin, V. Meunier, L. Cardenas, Y. F. Revurat, A. Cossaro, A. Verdini, D. F. Perepichka, F. Rosei and G. Contini, *ACS Nano*, 2013, **7**, 8190.

42 E. A. Lewis, C. J. Murphy, A. Pronschinske, M. L. Liriano and E. C. H. Sykes, *Chem. Commun.*, 2014, **50**, 10035.

43 Q. Sun and W. Xu, *ChemPhysChem*, 2014, **15**, 2657.

44 W. Xu, H. Kong, C. Zhang, Q. Sun, H. Gersen, L. Dong, Q. Tan and F. Besenbacher, *Angew. Chem., In. Ed.*, 2013, **52**, 7442.

45 M. Chen, J. Xiao, H. P. Steinrück, S. Wang, W. Wang, N. Lin, W. Hieringer and J. M. Gottfried, *J. Phys. Chem. C*, 2014, **118**, 6820.

46 C. Zhang, Q. Sun, H. Chen, Q. Tan and W. Xu, *Chem. Commun.*, 2015, **51**, 495.

47 Q. Fan, C. Wang, Y. Han, J. Zhu, W. Hieringer, J. Kuttner, G. Hilt and J. M. Gottfried, *Angew. Chem., Int. Ed.*, 2013, **52**, 4668.

48 M. Bieri, S. Blankenburg, M. Kivala, C. A. Pignedoli, P. Ruffieux, K. Müllen and R. Fasel, *Chem. Commun.*, 2011, **47**, 10239.

49 L. Pinardi, G. Otero-Irurueta, I. Palacio, J. I. Martinez, C. Sanchez-Sanchez, M. Tello, C. Rogero, A. Cossaro, A. Preobrajenski, B. Gomez-Lor, A. Jancarik, I. G. Stara, I. Stary, M. F. Lopez, J. Mendez and J. A. Martin-Gago, *ACS Nano*, 2013, **7**, 3676.

50 Q. Sun, C. Zhang, Z. Li, K. Sheng, H. Kong, L. Wang, Y. Pan, Q. Tan, A. Hu and W. Xu, *Appl. Phys. Lett.*, 2013, **103**, 013103.